LA-UR-02-0556

Title: MAPPING RESIDUAL STRESSES AFTER FOREIGN OBJECT DAMAGE USING THE CONTOUR METHOD

Author(s): Michael B. Prime, LANL, ESA-WR
Rick L. Martineau, LANL, SNS-3

Submitted to: 6th European Conferences on Residual Stresses, July 10-13, 2002, Coimbra, Portugal
Proceedings to be published in Materials Science Forum

Los Alamos
NATIONAL LABORATORY

Form 836 (8/00)

Mapping Residual Stresses After Foreign Object Damage Using The Contour Method

Michael B. Prime[1*], Rick L. Martineau[1]

[1] Los Alamos National Laboratory, Los Alamos, NM, 87545 USA. *prime@lanl.gov

Keywords: HSLA-100 steel, impact, penetration, ballistic, residual stress, armor, projectile.

Abstract. A 51-mm thick plate of High-Strength Low-Alloy (HSLA-100) steel was impacted by a 6.4 mm diameter tungsten carbide sphere traveling at 2.2 km/sec. The projectile penetration left a 10 mm diameter and 12 mm deep crater. A residual stress map over a cross-section through the crater was measured by the contour method. The predominant feature of the stress map was a peak compressive stress of 900 MPa, or 1.3 times the yield strength, centered about 1½ crater radii below the crater floor. The results were compared with an explicit finite element simulation of the impact event. The model has good agreement with the measured residual stresses. As part of the study, residual stresses in the as-received HSLA-100 plate were also measured and found to be a typical quenching stress distribution with peak compressive stress of about 165 MPa a few mm below the surface and tensile stress of 200 MPa in the center of the plate thickness.

Introduction

Residual stresses caused by foreign object damage are receiving increased attention because of their affect on subsequent part performance. The term "foreign object damage" (FOD) originated to describe damage of the blades in jet aircraft turbine engines. Such damage is caused by impingement of debris, sand, hailstones, etc. High-cycle fatigue, the leading cause of failure of these engines, usually occurs in a region affected by foreign object damage [1]. The influence of residual stress on fatigue failures in other (non-FOD) situations has been well established [2]. However, fatigue failures in regions of FOD are affected by the additional factors of stress concentration, microstructural damage, and cracks formed during the impact event. Only recently have studies isolated residual stress effects and shown that they indeed play a major role in the observed degradation of fatigue life [3,4]. Although coined for turbine blades, the term "foreign object damage" is equally appropriate for other applications, and the interest in the resulting residual stresses is also quite relevant. For example, space structures are susceptible to high-velocity impact from debris, and residual stresses from a simulated space-structure impact event were experimentally shown to have a drastic effect on the fatigue crack propagation rate of a defect nucleated from the impact [5]. In the study reported in this paper of a plate penetrated by a projectile, the residual stresses are examined because of their possible effect on the ability of armor or a containment vessel to a) survive multiple impacts or b) to survive future service loads when the original impact event did not cause total failure.

By using the contour method, the study described in this paper was able to generate the first experimentally measured map of sub-surface residual stresses from FOD. The study also used a finite element model to predict the penetration size of the crater and also predict the resulting residual stresses. Only a few experimental measurements of the residual stresses left by foreign object damage have been reported in the literature, such as a fairly simple test to estimate the surface residual stresses after an impact event on an aluminum plate [5]. Recently, synchrotron X-ray diffraction [6,7] was used to examine residual strains in the region of a dynamic impact onto a plate of Ti-6Al-4V [8]. Although that study was the most extensive measurement to date of FOD residual stresses, only surface stresses were measured because of experimental limitations.

Specimen

Material. The plate material tested in this study was a low carbon, copper precipitation hardened, High-Strength Low-Alloy steel: HSLA-100. This steel is used for naval ship hulls, armor, and containment vessels. The chemical composition is given in Table 1. The 51 mm thick plate material was prepared by hot cross-rolling. It was Ausentized at 900 ºC for 75 minutes and then water quenched. The plate was then tempered at 660 ºC for 200 minutes followed by another water quench. Subsequent mechanical testing gave yield strengths of 690 MPa in the final rolling direction and 685 MPa in the transverse direction, with corresponding ultimate strengths of 813 MPa and 829 MPa, respectively. A flame cut section of plate measuring 148 mm wide and 457 mm long was used for the impact experiments described in this study.

Table 1. Chemical composition of HSLA-100 steel plate in wt-%

C	Mn	P	S	Cu	Si	Ni	Cr	Mo	V	Ti	Al
0.06	0.85	0.005	0.002	1.56	0.26	3.45	0.56	0.58	0.003	0.001	0.025

Tungsten carbide spheres with a 6.35 mm diameter were used as projectiles. The composition of the spheres is 94% tungsten carbide with 6% of a cobalt binder

Impact. The steel was impacted normal to the plate surface by the small diameter spheres with velocities ranging from 1.0-2.5 km/s. The projectiles were fired from a 0.50-inch caliber smooth bore gun after being placed in a polyethylene obturator that was specifically designed to release the projectile during flight. The velocity of the projectile was measured using a pair of light screens, which was placed between the gun and target. An angled stripper plate was located between the light screens and target to further separate the projectile from the obturator. The impact events were spaced a minimum of one plate thickness (51 mm) from each other along the 457 mm length of the test piece, see Figure 1, and both of the 457 mm × 148 mm faces were used for tests. The particular impact event examined in this study was a 2.2 km/sec impact. Figure 2 shows a cross-section of that impact crater. The crater was approximately 10 mm in diameter and 12 mm deep at its center relative to the top of the piled-up region around the crater, which is about 3.6 mm above the undeformed surface.

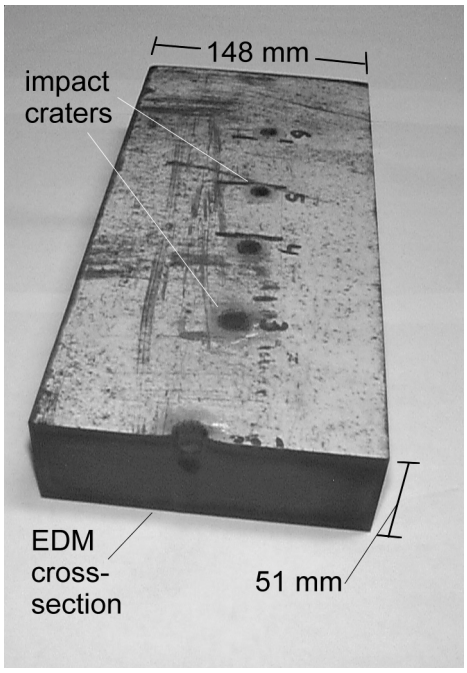

Figure 1. Plate used in impact experiments, showing multiple crates and EDM cut used to measure residual stress,

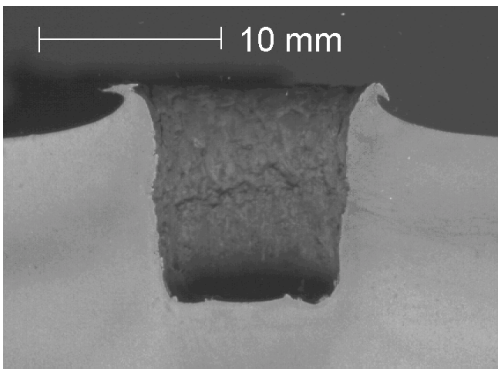

Figure 2. Cross-section of impact crater.

Residual Stress Measurement

Contour Method. The recently introduced contour method [9,10] maps residual stresses using two experimental steps followed by an analytical step. First, the part of interest is carefully cut in two with a precise, flat cut. The part relaxes as the cutting releases the residual stresses. The surface of the cut, assuming the cut was made on a made on a flat plane, deforms into a shape, or contour,

which is uniquely related to the original residual stresses. Therefore, the second experimental step is to measure the contour of the cut surface. Finally, a simple finite element analysis using Bueckner's Superposition Principle [11] will convert the measured surface contour back into a map of the original residual stresses. The ability of the contour method to accurately measure a complex stress map has been experimentally validated by comparison with neutron diffraction measurements on a welded plate [12], and the method has proved relatively simple to use [e.g., 13].

The Cut. For this test, the plate was cut with a Mitsubishi FX-10 wire Electric Discharge Machine (EDM) and a 150 μm diameter brass wire. The test piece was cut through the center of the penetration crater, see Figure 1, making a cut surface approximately 51 mm × 148 mm. "Skim cut" settings, which are normally used for better precision and a finer surface finish, were used because they also minimize any recast layer and cutting-induced stresses [14]. To prevent the cut from deviating from the original cut plane, a fixture was constructed to clamp the specimen on both sides of the cut during the cutting. It took almost 13 hours to complete the 148 mm long cut, but this time poses no problem because the EDM machine can be left to run overnight.

Surface Contour Measurement. After cutting, the plate was removed from the clamping fixture. The contours of both cut surfaces were measured using a MS Impact II coordinate measuring machine (CMM), an inspection tool that uses a touch trigger probe. A 1 mm diameter spherical ruby tip was used on the probe. The cut surfaces were measured on a 0.5 mm spaced grid, giving about 29,000 points on each cut surface.

Figure 3 shows data points measured on one of two halves after cutting. The peak-to-valley range in the contour is about 150 μm. The most striking feature in the contour is the large bump centered about 1 diameter below the impact crater.

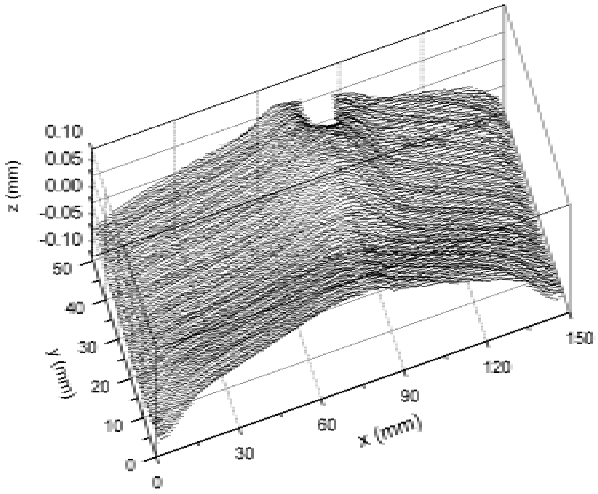

Figure 3. Surface contour measured by the Coordinate Measuring Machine after cutting specimen.

A test cut was used to validate the assumption of a flat cut. The EDM test cut was made near the edge of the specimen where the free surface condition would indicate that the stresses should be less than 10% of the values expected in the central region of the specimen. The contour subsequently measured on the test cut surface was less than 6 μm peak-to-valley, which is consistent with the stresses expected in this region and validates the assumptions.

Stress Calculation. The residual stresses were calculated from the measured surface contours using a finite element (FE) model. A 3-D model was constructed of one half of the plate, the condition after it had been cut in two, including the crater as a pre-existing feature. The mesh was graded with a minimum element size of about 1 mm, resulting in 116,980 linear shape–function (i.e., 8 node) brick elements and 375,408 degrees of freedom. The material behavior was isotropic elastic with an elastic modulus of 197 GPa and Poisson's ratio of 0.29.

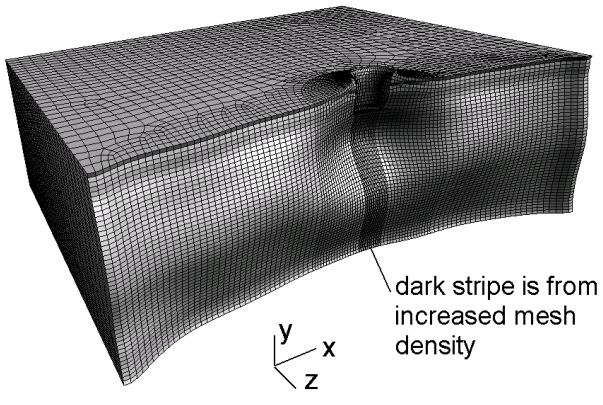

Figure 4. Finite element model after applying displacement boundary condition to cut surface.

In order to smooth out noise in the measured surface data and to enable evaluation at arbitrary locations, the data were fitted to bivariate

Fourier series. The bivariate Fourier series fits to the measured contour data were evaluated at a grid corresponding to the FE nodes, averaged between the two sides, and then applied as *z*-direction displacement boundary conditions. Three additional displacement constraints were applied to prevent rigid body motions. Figure 4 shows the deformed FE model. The surface stresses were then obtained by evaluating the values of σ_z at the nodes of the surface elements and averaging among all elements sharing a given surface node.

Model

The explicit finite element calculation of the dynamic impact was performed using LS-DYNA, a commercially available Lagrangian finite element code [15]. An axisymmetric finite-element model of the plate and sphere was crated using 4-node elements. The mesh for the ball consisted of 467 elements with an element size of approximately 0.2 mm. The mesh for the plate consisted of 22500 elements, with a graded distribution. The smallest elements, which were nearest the point of impact, had a minimum element size of 0.4 mm.

Both materials used the elastic plastic hydrodynamic material model (Mat 10) with an Equation of State (EOS). The rate dependent flow stress data for the HSLA material were determined from Hopkinson-bar testing performed at LANL [16]. The physical properties and ultimate strength of the spheres were based on published data [17]. Failure strains of 0.8 and .007 were respectively defined for the plate and sphere materials. In addition, the spall option was activated for the tungsten carbide. The time step for the analysis was 2 nanoseconds. To achieve a reasonable steady state in the residual stresses, the calculation was continued to 52 ms. An enlarged image illustrating the experimentally observed crater from the 2.2 km/s impact is shown in Figure 2 and a comparison of the crater shapes obtained from the finite element model and experiment is shown in Figure 5.

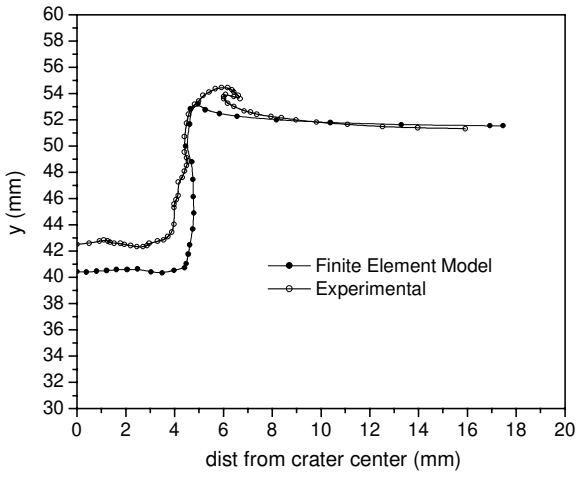

Figure 5. Measured and calculated crater shape from 2.2 km/s impact.

Results

Figure 6 shows the map of residual stress (σ_z) measured by the contour method, and Figure 7 shows the prediction from the finite element model, where the hoop stress in the axisymmetric model corresponds with the measured σ_z. Good agreement between the model and the measurements is especially evident in the region of compressive stress centered about 2 crater radii below the bottom of the crater. The size and shape of the compressive region is similar between the prediction and the measurement. The model predicted a peak compressive stress of 1100 MPa and the measurements gave a value of about 900 MPa. Considering the highly nonlinear nature of the impact event and the large range of strain rates and temperatures experienced during the impact, this agreement is excellent. Note that the peak compressive stress significantly exceeds the yield strength of about 690 MPa because the stress is highly triaxial in this region. For the element with the peak hoop stress of -1100 MPa, the model predicted radial stress of -696 MPa and y-stress of -896 MPa, which, combined with non-zero shear stresses, gives a Mises stress of only 500 MPa. Individual residual-stress components exceeding yield strength because of triaxiality has been observed routinely, usually in tensile stress regions of welds [2].

The agreement between the prediction and the measurement is less evident in other regions of the stress map because the test plate had initial residual stresses before the impact, and the model did not. Examination of Figure 6 reveals a background residual stress distribution of compressive stress near the top and bottom surfaces of the plate and tensile in the center, typical of quenching stresses.

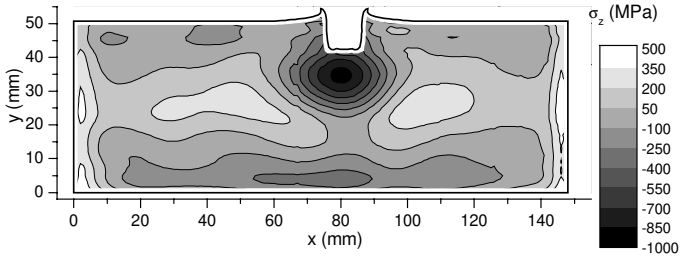

Figure 6. Measured residual stress map after projectile penetration.

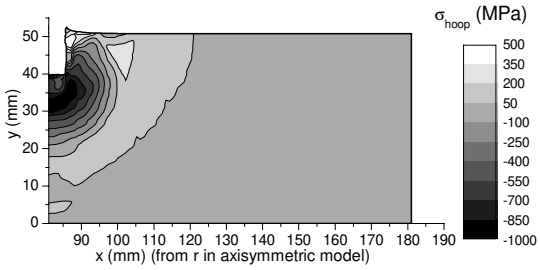

Figure 7. Residual hoop stress prediction from axisymmetric model, shown on half of cross-section.

To evaluate the effect of initial residual stresses, a stress map was measured on some HSLA-100 plate that had not been impacted. Because it was the only piece available, a 60.75 mm thick plate was tested using the contour method. This plate underwent the same processing and was expected to have very similar initial residual stresses to the 51 mm thick plate used in the impact tests. Figure 8 shows the measured stress map in the thicker plate, which shows the expected quenching distribution of residual stresses. Note that the stress map in Figure 8 does not show the same high tensile stresses at the $+x$ and $-x$ edges as Figure 6 because the specimen measured for Figure 8 was saw cut along those edges from a larger plate whereas the specimen used for Figure 6 had been flame cut. Flame cutting, not surprisingly, produced much higher stresses.

A subsequent coarse attempt to account for the initial residual stresses proved to be surprisingly effective at reconciling the model predictions with the measurements. Unfortunately, there is no convenient mechanism for introducing initial residual stresses into the explicit LS-DYNA simulation. Therefore, a correction was made to the measured stress map by subtracting off the initial residual stresses. Such a subtraction implies the stress maps can be superimposed, which obviously over-simplifies the highly nonlinear process. Nonetheless, the resulting stress map shown in Figure 9 agrees remarkably well with the model prediction of Figure 7.

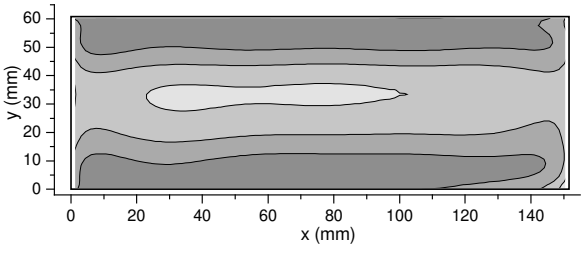

Figure 8. Residual stress map in as-received plate showing original quenching stresses.

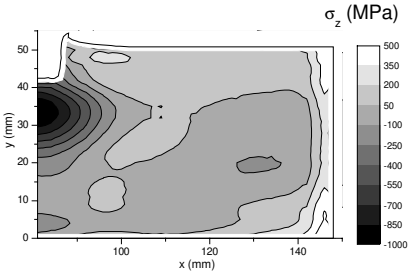

Figure 9. Measured *change* in residual stresses from impact event. Compare with Figure 7.

The distribution of residual stresses in the as-received plate may be useful for other applications of HSLA-100 steel. The specification for this material does not allow thermal stress relief [18] because of potential loss of strength. Therefore, such quenching stresses can be expected for all uses of this material. Away from the edges, the stress distribution in Figure 8 is primarily a 1-D through-thickness variation. Figure 10 plots the through-thickness stresses for the stress map in Figure 8,

excluding data within 30 mm of the edges. A symmetric fit of the data gives a good estimation of the stresses to within an uncertainty of about ±20 MPa. The fit is given by the equation

$$\sigma/S_y = 0.29 - 0.96\tilde{y}^2 - 3.371\tilde{y}^4 + 11.568\tilde{y}^6 - 12.179\tilde{y}^8 + 4.455\tilde{y}^{10},$$

where the through-thickness variable $\tilde{y}$ is normalized to go from –1 to +1 through the thickness of the plate and S_y is 690 MPa.

Conclusions

1. The complex cross-sectional residual-stress map in a penetrated plate was measured using the contour method. The stress map probably could not have been measured with any other technique [19]. For example, measuring a comparable stress map with neutron diffraction would not have been practical because of the 51 mm thickness of the plate.
2. The impact produced a region of compressive residual stress exceeding the material's yield strength, located about two crater radii below the crater floor, balanced by a region of tensile stresses located farther from the crater. The tensile stresses would be of special concern for subsequent material failures, especially because the tensile region reaches to the part surface, a likely area for crack initiation.
3. The explicit finite-element model gave reasonable agreement with the measurements but over-predicted the depth of penetration and the residual-stress magnitudes.
4. The model predictions could probably be improved if the initial residual stresses in the plate were accounted for.

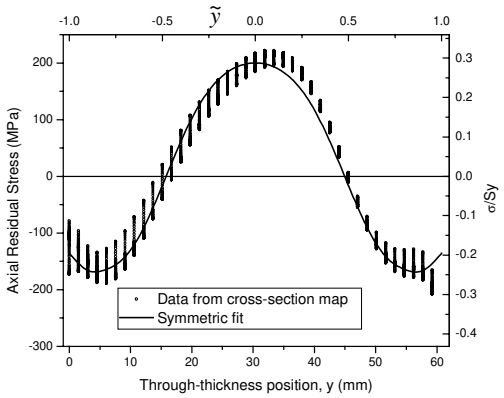

Figure 10 Through-thickness variation of residual stresses in as-received HSLA-100 plate.

Acknowledgement

This work was performed at Los Alamos National Laboratory, operated by the University of California for the United States Department of Energy under contract W-7405-ENG-36.

References

[1] B.A. Cowles: Int. J. Fract., Vol. 80 (1996), pp. 147-163.
[2] G. A. Webster and A. N. Ezelio: Int. J. Fatigue, Vol. 23 (2001), S375-S383.
[3] S. Mall, et al.: Mech. Mater., Vol. 33 (2001), pp. 679-692.
[4] S. R. Thompson, J. J. Ruschau and T. Nicholas: Int. J. Fatigue, Vol. 23 (2001), S405-S412.
[5] A. Laciotti and S. Ottavio: Fatigue Fract. Engng Mater. Struct., Vol 24 (2001), pp. 419-427.
[6] W Reimers et al.: J. Nondes. Eval., Vol. 17 (1998, pp. 129-140.
[7] P. J. Webster et al.: J. Strain Anal. Eng. Des., Vol. 36 (2001), pp. 61-70.
[8] B.L. Boyce, et al.: Mech. Mater., Vol. 33 (2001), pp. 441-454.
[9] M.B. Prime: J. Engng. Mater. Tech., Vol. 123 (2001), pp. 162–168.
[10] http://www.lanl.gov/contour/
[11] H.F. Bueckner: Trans. Amer. Soc. Mech. Engineers, Vol. 80 (1958), pp. 1225–1230.
[12] M.B. Prime, D.J. Hughes and P. J. Webster: Proc. 2001 SEM Annual Conf. on Experimental and Applied Mechanics, June 4-6, Portland, OR, pp. 608-611.
[13] I. Virkkunen: Doctoral Disertation, Helsinki U. Tech., Nov. 2001.
[14] W. Cheng, et al.: J. Engng. Mater. Tech., Vol. 116 (1994), pp. 556–560.
[15] LS-DYNA Version 950, Users Manual, Livermore Software Technology Corporation, June 1997.
[16] S. R. Chen, private communication.
[17] A. E. Johnson, Jr., National Advisory Committe for Aeronautics, Technical Note 3309, (1954)
[18] MIL-S-24645A(SH), United States Navy (1990) .
[19] P.J. Withers and H.K.D.H. Bhadeshia: Mat. Sci. & Tech., Vol. 17 (2001), pp. 355-365.